Supplement of Atmos. Meas. Tech., 18, 7187–7220, 2025 https://doi.org/10.5194/amt-18-7187-2025-supplement © Author(s) 2025. CC BY 4.0 License.





## Supplement of

## Closing the gap: an algorithmic approach to reconciling in-situ and remotely sensed aerosol properties

Joseph S. Schlosser et al.

Correspondence to: Joseph S. Schlosser (joseph.schlosser@hamptonu.edu)

The copyright of individual parts of the supplement might differ from the article licence.

## **Supplementary Material**

The supporting information includes five figures and three tables to complement the main manuscript's external consistency analysis.

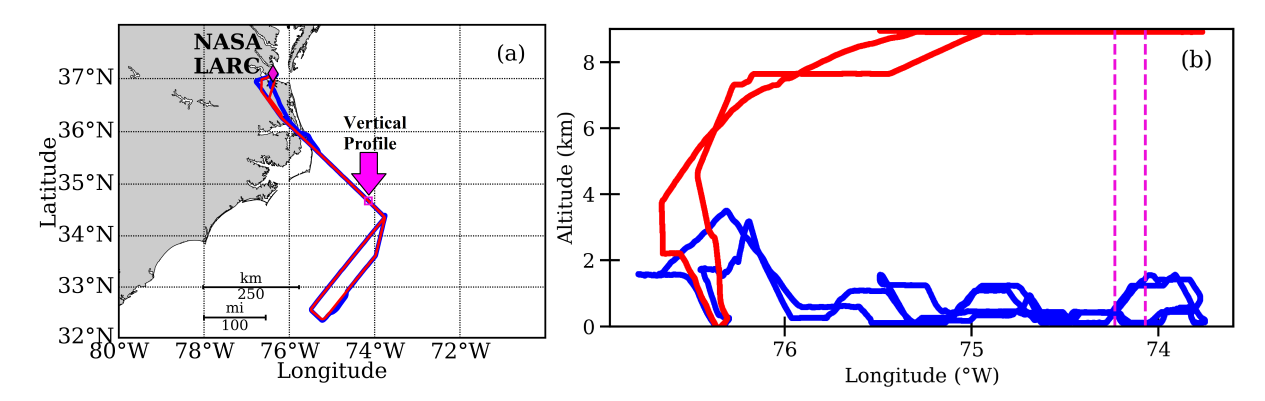


**Figure S1.** (a) Top-down and (b) longitudinal views of the Falcon and King Air flight tracks from Research Flight 158 that occurred on 20 May 2022. The blue and red lines represent the Falcon and King Air flight paths, respectively. The location of the Case 9 is bounded by the magenta box in panel (a) and by the vertical dashed lines in panel (b).



**Figure S2.** NASA Worldview satellite image of fire presence (red points) during Research Flight 158 (20 May 2022) case flight with locations of LaRC and the Falcon flight spiral labeled. This image is used to identify sources of smoke on this day and comes from the VIIRS Fire and Thermal Anomalies product available from the NOAA-20 satellite (Schroeder et al., 2014).

## NOAA HYSPLIT MODEL Backward trajectories ending at 1400 UTC 20 May 22 NAM Meteorological Data

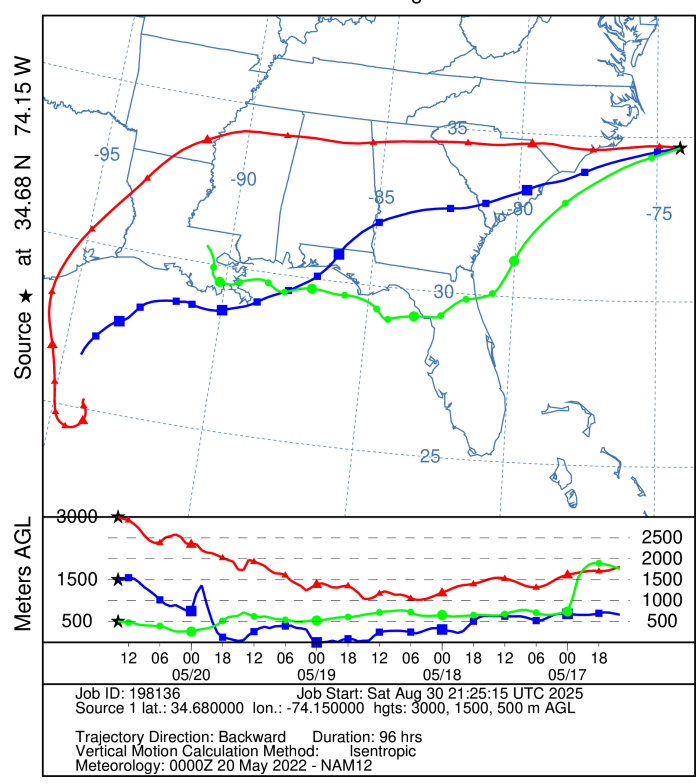


**Figure S3.** Four-day Hybrid Single Particle Lagrangian Integrated Trajectory model (HYSPLIT) back trajectories end at the altitudes of 0.5, 1.5, and 3 km above sea level, at 14:00 UTC on 20 May 2022, and at the location of Case 9 from Research Flight 158.

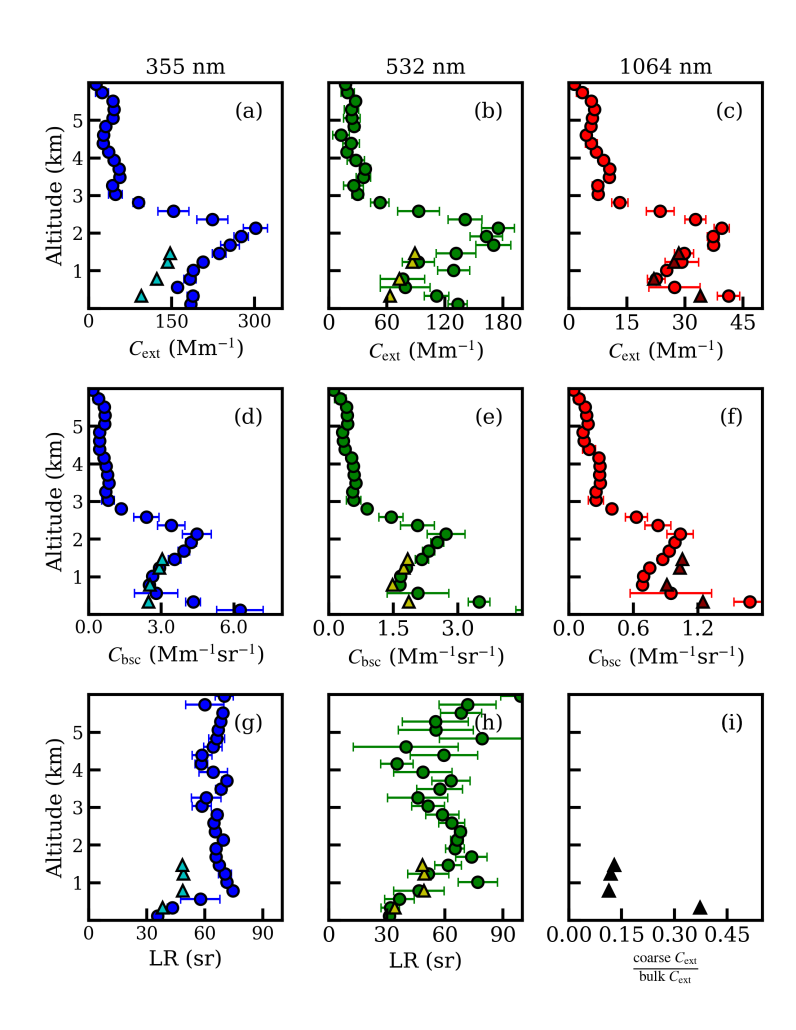


Figure S4. Vertical profiles of HSRL-2-derived (circles) and ISARA-derived (triangles) ambient  $C_{\rm ext}$  at (a) 355 nm, (b) 532 nm, and (c) 1064 nm wavelengths,  $C_{\rm bsc}$  at (d) 355 nm, (e) 532 nm, and (f) 1064 nm wavelengths, LR at (g) 355 nm and (h) 532 nm wavelengths, and (i) the ratio of coarse extinction to bulk extinction at 532 nm from Case 9 that occurred during Research Flight 158 on 20 May 2022. The error bars shown indicate the standard deviation of a given aerosol property.

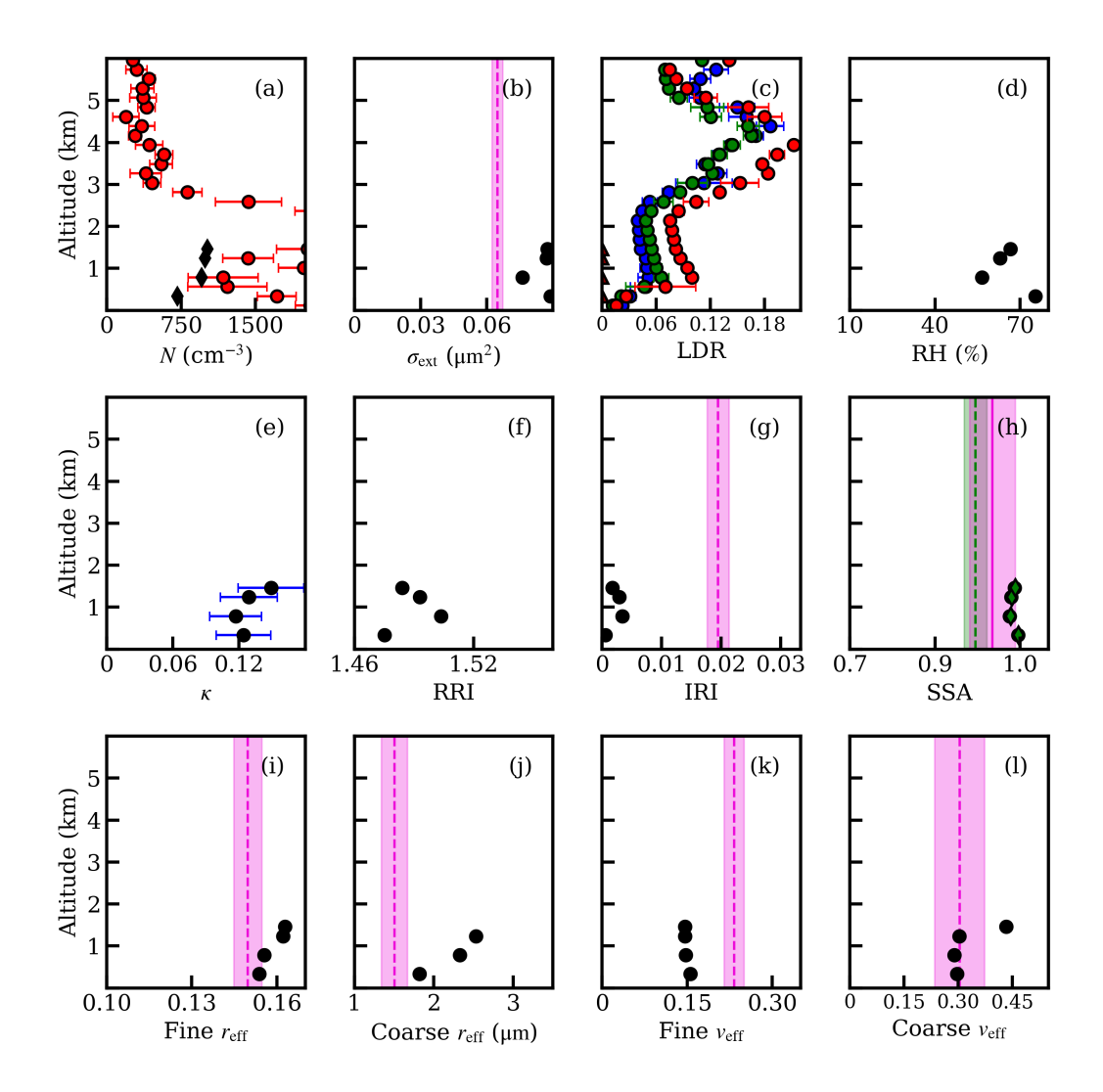


Figure S5. Vertical profiles of (a) RSP+HSRL-2-derived (red points) and ISARA-derived (black points) N, (b) ISARA-derived optical  $\sigma_{\rm ext}$  at 532 nm, (c) LDR derived from HSRL-2 (circles) and ISARA (triangles) at 355, 532, and 1064 nm (d) in-situ-measured ambient RH, along with ISARA-derived (e)  $\kappa$ , ambient (f) RRI, (g) IRI, (h) fine (green diamonds) and total (black diamonds) SSA, (i) fine effective radius ( $r_{\rm eff}$ ), (j) coarse  $r_{\rm eff}$ , (i) fine effective variance ( $v_{\rm eff}$ ), and (j) coarse  $v_{\rm eff}$  from Case 9. The dashed magenta lines and shaded regions on panels (b) and (f)–(i) are the column-averaged properties and their associated uncertainties derived from the RSP. Panel (h) has an additional green dashed line and shaded region that represents the fine SSA derived from the RSP. The error bars shown indicate the standard deviation of a given aerosol property. Where available, the blue error bars indicate the uncertainty of an aerosol property as given from the synthetic consistency analysis. The ISARA-, HSRL-2- and RSP-derived total AOD are 0.09, 0.45 and 0.45, respectively.

**Table S1.** Consistency statistics that result from the comparisons of altitude-resolved spectral  $C_{\rm ext}$ ,  $C_{\rm bsc}$ , and LR, as well as N. The consistency statistics shown correspond to the vertical profile from for Case 9 shown on Figures S4 and S5a.

Aerosol		bias		relative bias (%)		NRMSD			
Property	$\lambda$ (nm)	MB	SB	MRB	SRB	(%)	r	p	count
$C_{ m ext}~({ m Mm}^{-1})$	355	76	17	47	13	55	0.75	0.25	4
	532	25	24	26	25	47	0.28	0.72	4
	1064	3	3	8	7	20	0.98	0.02	4
$C_{\rm bsc}~(\mathrm{Mm}^{-1}\mathrm{sr}^{-1})$	355	0.58	0.87	17	26	52	-0.13	0.87	4
	532	0.55	0.73	23	26	42	0.68	0.32	4
	1064	-0.06	0.34	-12	29	30	0.94	0.06	4
LDR	355	0.04	0.01	200	0	86	-0.59	0.41	4
	532	0.05	0.02	200	0	80	-0.30	0.70	4
	1064	0.07	0.03	200	0	79	0.29	0.71	4
LR (sr)	355	18	9	31	13	54	0.98	0.02	4
	532	3	7	4	14	23	0.84	0.16	4
Optical $N \text{ (cm}^{-3})$	-	666	403	51	28	57	-0.08	0.92	4

Table S2. Ambient optical and microphysical aerosol properties for Case 9 derived from the ISARA and the RSP. Ambient aerosol properties compared include the column-averaged properties of RRI, IRI, fine- and coarse  $r_{\rm eff}$  and  $v_{\rm eff}$ , optical N and  $\sigma_{\rm ext}$ , as well as spectral (355, 532, and 1064 nm) SSA for both the fine and the total aerosol. The ISARA-derived extinction weighted average properties are shown with the weighted standard deviation and the RSP-derived properties are shown with the expected error from published sources where the measurement uncertainty was not available. The RSP retrieved fine- and coarse AOD at 532 nm for this case is shown on Table 3.

Aerosol	ISA	ARA	RSP		
Property	$ar{Z}_{ ext{weight}}$	$s_{ m weight}$	column	uncertainty	
Fine $r_{\rm eff}$ (µm)	0.16	0.00	0.15	0.01	
Fine $v_{\rm eff}$	0.15	0.00	0.23	0.02	
Coarse $r_{\rm eff}$ ( $\mu$ m)	2.65	0.66	1.50	0.16	
Coarse $v_{ m eff}$	0.34	0.06	0.3	0.07	
Fine RRI	1.49	0.01	1.60	0.02	
Fine IRI	0.002	0.001	0.018	0.002	
Optical $\sigma_{\rm ext}$ at 532 nm ( $\mu m^2$ )	0.08	0.01	0.06	0.002	
Optical $N$ (cm <sup>-3</sup> )	933	114	3028	196**	
Fine SSA at 355 nm	0.99	0.00	0.92	0.02*	
Bulk SSA at 355 nm	0.99	0.01	0.94	0.04*	
Fine SSA at 532 nm	0.99	0.00	0.92	0.02*	
Bulk SSA at 532 nm	0.99	0.01	0.95	0.04*	
Fine SSA at 1064 nm	0.98	0.01	0.88	0.02*	
Bulk SSA at 1064 nm	0.99	0.01	0.97	0.04*	

<sup>\*</sup> Stamnes et al. (2018)

<sup>\*\*</sup> Schlosser et al. (2022)

**Table S3.** Consistency statistics resulting from the comparisons of the altitude-resolved aerosol properties of spectral  $C_{\rm ext}$ ,  $C_{\rm bsc}$ , and LR, as well as N. The consistency statistics shown correspond to the unfiltered data set. The unfiltered data set are shown as gray circles in the scatterplots shown on Fig. 15.

Aerosol		bias		relative bias (%)		NRMSD			
Property	$\lambda$ (nm)	MB	SB	MRB	SRB	(%)	r	p	count
$C_{ m ext}~({ m Mm}^{-1})$	355	30	32	44	42	19	0.81	0.00	83
	532	15	21	34	52	18	0.70	0.00	98
	1064	1	11	9	55	20	0.44	0.00	99
$C_{ m bsc}~({ m Mm}^{-1}{ m sr}^{-1})$	355	0.7	0.8	45	56	19	0.72	0.00	83
	532	0.4	0.6	31	53	17	0.69	0.00	99
	1064	0.01	0.45	-3	62	16	0.59	0.00	99
LDR	355	0.08	0.04	172	46	35	0.80	0.00	70
	532	0.06	0.03	162	64	32	0.69	0.00	88
	1064	0.07	0.06	143	80	33	0.53	0.00	75
LR (sr)	355	-1	20	-7	40	21	0.30	0.01	75
	532	3	18	-1	43	22	0.43	0.00	91
Optical $N$ (cm <sup>-3</sup> )	-	135	584	0.5	69	21	0.46	0.00	98